Journal of Natural Sciences and Mathematics (JNSM)
Vol. 15, pp 35-53 (January 2022)

Synthesis, characterization of Lanthanum mixed ligand complexes based on benzimidazole derivative and the effect of the added ligand on the antimicrobial, and anticancer activities.

S. El-Sayed Saeed [*1] and Ahmed N. Alhakimi[1,2]

[1] Department of Chemistry, College of Science, Qassim University, Buraidah 51452, Saudi Arabia.
[2] Department of Chemistry, College of Sciences, Ibb University, Yemen.
* Correspondence: s.saeed@qu.edu.sa or saiedelsayed2@yahoo.com

Abstract:

Primary Schiff Base of lanthanum (III) benzimidazole complex (2) [La(L)Cl_2(H_2O)] has been synthesized by condensation of the major ligand 2-(1H-benzimidazol-2-ylmethyliminomethyl) phenol (HL) (1) with lanthanum (III) chloride. The mixed ligand complexes were prepared with the reaction of salicylaldehyde or furfural aldehyde as bidentate and ammonia as a monodentate ligand with the main complex (2). The ligand, the major complex, and the mixed ligand complexes 2-5 were verified by elemental analysis, molar conductivity, spectral measurements (IR, ^{1}H,^{13}C-NMR, UV), and thermo-gravimetric analysis. The ligand (1) behaves as a mono-negative tridentate compound. The oxygen atom of the phenolic group, the azomethine atom, and the Penta ring nitrogen atom benzimidazole was connected to lanthanum. This bonding relationship was unchanged in all of the mixed ligand lanthanum complexes. Antimicrobial and anticancer effects were analyzed *in vitro* biological studies. To evaluate the *in vitro* antitumor activity in HEPG2 liver and HCT116 colon cancer cell lines, the effects of ligand 1 and mixed ligand complexes 2-5 were studied. Compared with ampicillin and amphotericin B, the prepared ligand and complexes showed antibacterial and antifungal activities. The ligand and complexes exerted cytotoxicity on the HCT116 cell line superior to that observed with the HEPG2 cell line.

Keywords:
Lanthanum mixed ligand; benzimidazole derivative; HEPG2 and HCT116 antitumor activities

Introduction

Heterocyclic compounds play a large effect in medicinal chemistry due to their huge biological action. Their varied pharmacological profile, sulfur, oxygen, and nitrogen-containing heterocyclic compounds still attract chemists and researchers' attention in several areas [1-4]

One of the heterocyclic compounds is benzimidazole, heterocyclic group variation of these compounds shows antimicrobial activity that inhibits microbial diseases [5], an anti-tuberculosis activity that is influential against tuberculosis [6], anticancer action that slows or avoids cancer [7], as an antiparasitic drug that extracts the worms of parasites (helminths) and other internal parasites from the host without causing side effects to the body [8]. It also can be used as an anti-allergic compound that momentarily helps reduce allergic reactions symptoms [9] and as an anti-oxidant, the proteins oxidation, lipids, DNA, or other molecules by blocking the spread stage [9]. They also are noted for their anti-inflammatory (swelling, redness, and pain) [10], antibacterial [11, 12], and antifungal activities [13]. Schiff bases molecules contain a molecular group of imine or azomethane (–C=N–). These are primary amines condensation with carbonyl compounds, first mentioned by Hugo Schiff [14]. Schiff bases represent essential classes of organic compounds most widely used in a broad variety of applications, including analytical, biologic, and inorganic chemistry.

Complexes of Schiff base have gained prominence in pharmaceutical and therapeutic fields due to a broad biological activity such as anti-inflammatory [15], analgesic [10], anthelmintic [16], antimicrobial [17], anticancer [18], anticonvulsant, anti-tuberculosis [19], antioxidant [20], etc. The azomethine nitrogen atom can form hydrogen bonds with active cell centers constituents and may interfere with normal cell processes [21].

Transition metals compounds and composites have antimicrobial behaviors and are used as photocatalytic activity [22, 23], luminescent nanomaterials [24, 25], and conductivity enhancement [26].

The continued interest of the Schiff bases studies [13] and the previous significance about the mixed ligand of benzimidazole Schiff base has inspired us to investigate the complexes mixed ligand benzimidazole Schiff base derivative. The proposed work aims to design and synthesize new Schiff base complexes based on benzimidazole of substituted aryl and study their anticancer and antimicrobial activities.

2. Experimental

2.1 Chemicals

The reagents which used in the ligand and its complexes synthesis were provided by Sigma-Aldrich Company.

2.2 Instruments

Elemental analysis (CHN) was carried out in Cairo University (Egypt), Micro Analytical Centre. The content of metal and chloride ions were analyzed using Standard analytical methods [27]. IR spectra of benzimidazole Schiff Base HL and its metal complexes were carried out by using JASCO - IR 4700 spectrophotometer with KBr as supporting content and scanned from 400 to 4000 cm^{-1} in ATR mode. The electronic absorption spectrum was recorded on Visible Spectrophotometer UV-1650 PC Shimadzu

spectrophotometer in the range 200-800 nm using ethanol as solvent. The ^{1}H- and ^{13}C-NMR spectra were recorded with Burker High-Performance Advance III 400 MHz FT-NMR spectrometer. The used solvent was deuterated dimethyl sulfoxide (d_6-DMSO). The thermal analyzer Shimadzu DT-30 was used to carry out thermal analysis (TG) from room temperature to 800 ºC at a heating rate of 10 ºC / min. Gouy Matthey Balance was used to test the magnetic susceptibility at 25 ° C and was determined using the known equation. Corrections of diamagnetic based on Pascal's constants were evaluated. Conductivity Bridge of the Tacussel type CD6NG was used to record the molar conductivity of 10^{-3} Molar solutions (DMF). According to the published equation, the molar conductivities measured in $\Omega^{-1}cm^2mol^{-1}$. Crystallinity and phase structure of the materials was performed using an X-ray diffractometer (Shimadzu6000-XRD) using CuK_α radiation ($\lambda = 1.54056$ Å).

2.3. Antimicrobial activity

Antimicrobial activity of the tested samples against Gram (–) *Escherichia coli*, G (+) *Staphylococcus aureus*, *Candida albicans*, and *Aspergillus flavus* was performed at the Micro Analytical Center in Cairo University, Egypt. By using a diffusion method of modified Kirby-Bauer disc [28]. In short, 100 microliters of test bacteria were cultured in 10 milliliters of freshly prepared media until the fungi had about 10^8 cells/ml or 10^5 cells/ml. 100 microliters of these suspensions were taken and applied to plates of agar equivalent to the broth in which they were kept alive. Each organism of isolated colonies that should be pathogens were picked from primary agar plates and monitored for dispersion process sensitivity. Plates inoculated with *Staphylococcus aureus* Gram (+) bacteria; *Escherichia coli* Gram (-) bacteria were incubated at 35-37 ºC for 24-48 h. The *Candida albicans* yeasts were incubated for 24-48 h at 30 ºC; filamentous fungi *Aspergillus flavus* for 48 h at 25 ºC. After that, the inhibition zones diameters were measured in millimeters [29]. Amphotericin B (antifungal agent) standard disks were used as a positive control and Ampicillin was used for the antibacterial positive action. Dimethyl sulfoxide (DMSO, 10 µl) solvent impregnated filter disks were used as negative controls. 10µM of the concentration of Stock solutions were tested by impregnation of 8.0 mm diameter blank paper disks. The tested compounds of the ligand and complexes disperse into agar from the filter paper disk impregnated with it; the chemical is diffused just around the disk in the agar. The solubility and the molecular scale of the chemical determine the size of the region around which the disk is penetrated. When an organism is put on the agar, it will not develop if it is sensitive to the chemical in the region around the disc. This disk region of no growth is known as the "inhibition zone" or the "clear zone". The diameters of the zone were determined with slippers of the Standards of National Committee for Clinical Laboratory [29]. Agar-based techniques like disk diffusion and E test can be good substitutes since they are easier and quicker than methods of breeding [30].

2.4. Anticancer activity

Cell lines and culturing; Cell lines of liver HEPG2 and colon HCT116 Human tumor carcinoma used in this study were supplied from the American Type Culture Collection

(ATCC, Minnesota, U.S.A.). The tumor cell lines were maintained by serial sub-culturing at the National Cancer Institute, Cairo, Egypt. The ligand and complexes samples were produced by dissolving 1:1 stock solution and stored at 20°C in DMSO.

The preparation of buffers and reagents was as follows:
For the maintenance and culturing of human tumor cell lines, 10% fetal bovine serum supplemented RPMI-1640 medium, containing 1% penicillin/streptomycin was used. The powder was applied to the medium. Dissolved 10.4 grams of powder and 2 grams of $NaHCO_3$ in 1 liter of distilled water, and the working solution formed. Sterilization of the medium was carried by filtrations in a Millipore bacterial filter (0.22 μm). After preparing the medium, it is kept in the refrigerator (4 ºC). Before using the medium, it was warmed at a water bath (37 ºC), supplemented by 10 % fetal bovine serum, and 1 percent penicillin/streptomycin were applied to the water bath at 37 ºC. Cell viability was determined by using 0.05% Trypan blue dye. Porcine Trypsin-EDTA 0.25 % solution was used to harvest the cells. The steps for maintenance, collection, determination, counting, and cryopreservation of the cell lines were carried out as described by Skehan [31].
Sulphorhodamine-B (SRB) assay according to the procedure by Vichai and Kirtikara was used to determine the cytotoxicity of the chemical on the human cancer cell lines [32]. SRB is an aminoxanthrene dye that has two sulfonic groups and light pink color. It is a protein stain that binds in mildly acidic conditions to amino groups of intracellular proteins to provide a sensitive cellular protein index. SRB with a concentration of 0.4 % was dissolved into 1 % acetic acid for use as a protein-dye. Anticancer activity assay was carried out according to this procedure:
Usually, procedures are not listed; the steps to be followed are written within a single paragraph such as the following:
Cells (3×10^3 /well) were seeded in 96-well microtiter plates 150 μl of freshly prepared culture medium and left for 24 hours to adhere to the plates. Then, different concentrations of drugs were added (0, 5, 12.5, 25, 50 μg/ml) in triplicate and the plates were incubated for two days. At the end of this period, 50 μl of cold 10% trichloroacetic acid were added to each well and further incubate for 1 h at 4 ºC. Plates were washed with distilled water (Automatic washer, Tecan, Germany), and then stained at room temperature with 50 μl of 0.4 % SRB in 1 % acetic acid for 30 min. Plates were washed again with 1% acetic acid and then dried with air. The dye incorporated by the cells was solubilized with 100 μl/well of 10 M Tris base (pH 10.5) and spectrophotometrically measured at 570 nm using an ELISA microplate reader (Sunrise Tecan reader, Germany). The average background absorption was immediately eliminated, and the median values were determined for each chemical drug concentration. The assay was done three times. The cell survival percentage was determined accordingly:

Surviving fraction = O.D. (cells are treated)/O.D. (cell control).

The IC50 values were also measured (resveratrol concentrations required to achieve inhibition of cell growth of 50%).

3. Method

3.1 Preparation of major ligand (HL) (1)

The synthesis of ligand 2-(1*H*-benzimidazol-2-ylmethyliminomethyl) phenol (HL) **(1)** was produced in the reported literature [33]. 2-aminomethylbenzimidazole dihydrochloride (2.20 g, 10 mmol) was dissolved in 30 mL of water and neutralized by adding aqueous K_2CO_3 solution (1.66 g, 12 mmol). A stirred salicylaldehyde solution (1.22g, 10 mmol) in 16 mL of methanol was added dropwisely to the above-described solution with stirring of 1 h. The yellow precipitation slowly formed. The precipitation was then filtered, washed thoroughly with water followed by petroleum ether, and dried in a vacuum.

80 %. Yield, m.p. 126^0 C: $C_{15}H_{13}N_3O$ (FW= 251.11) calculated: C, 71.7 %; H, 5.21%; N, 16.72% found: C, 71.5 %; H, 5.18%; N, 16.61%.

FT-IR (KBr, disc cm^{-1}, υ_{max}/ cm^{-1}) for **(HL) (1)** IR (KBr, υ): 3415, 3263, 1635, 1550, 1350 cm^{-1}. UV-Visible (DMF, λ_{max}): 422, 319, 273 nm. ^{1}H-NMR (400 MHz, DMSO-*d6*): *δ* 14.20 (d, 1H, ArOH), 12.70 (s, 1H, NH imidazole), 9.30 (s, 1H, N=CH), 6.80–8.12 (d, m, 10H, Ar-H), 5.11 (s, 2H, CH_2) ppm. ^{13}C-NMR (400 MHz, DMSO-*d6*) *δ*: 50.13, 107.01, 112.10, 119.12, 119.50, 123.45, 124.60, 126.05, 128.90, 129.60, 134.30, 134.70, 138.10, 151.12, 161.50, 175.70 ppm [34].

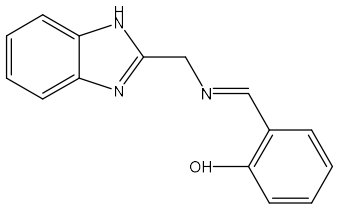

Structure of 2-(1*H*-benzimidazol-2-ylmethyliminomethyl) phenol HL (1)

3.2 Synthesis of metal complex

The preparation of the complexes was produced in two stages; the first stage was the synthesis of the main (benzimidazole Schiff Base) complex (2) [La (L) Cl_2 (H_2O_2). The second stage was the synthesize of mixed ligands by the reaction of the main complex with ammonia, furfural (Fur), or salicylaldehyde (Sal) as a secondary ligand.

3.2.1 Synthesis of the main (benzimidazole Schiff Base) complex (2) [La (L) Cl_2 (H_2O_2)]

The solution of Lanthanum (III) chloride (1mmol, 0.245 g) in 25 ml of ethanol was added dropwise to the magnetically stirred solution of primary ligand (1mmol, 0.251g) in 25 ml ethanolic solution. The mixture was stirred and refluxed for 6 hours. The canary yellow precipitate has been washed with ethanol and then dried with a vacuum. Yield: 74.5%. The complex $C_{15}H_{14}N_3O_2Cl_2La$ (FW= 478.10) elemental analysis calculated: H, 2.95%; C, 37.68 %; N, 8.79% found: H, 2.81%; C, 37.52 %; N, 8.41%. FT-IR (KBr, disc cm^{-1}, υ_{max}/ cm^{-1}) for the complex, 3358 (H_2O), 3267 (N-H), 3048-2665 (NH…O), 2125 (C-O) phenyl, 1617 (C=N) azomethine, 11611 (C=N) ring, 750 (La←N), 674 (La-O), and 432 (La-Cl). ^{1}HNMR (ppm DMSO-d_6): δ 8.53 (s, 1H, CH=N), 7.14–7.38 (m, 8 ArH), δ 4.0 (s, 2H, CH2-N). ^{13}C NMR (ppm d6-DMSO): δ 115.75–143.12 (Ar carbons), 164.18 (HC=N), 160.36 (C-O), 61.25 (CH_2) [35].

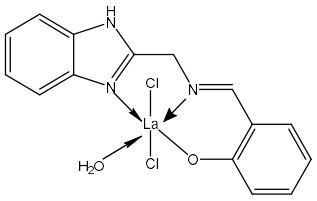

Structure of Benzimidazole Schiff Base Complex (2)

3.2.2 Synthesis of mixed ligand complexes

The ethanolic solution (1 mmol, in 25 ml of ethanol) of the complex (2) (benzimidazole Schiff Base) $[La(L)Cl_2(H_2O)]$ was condensed with (1 mmol, in 25 ml of ethanol) of ammonia, furfural (Fur), or salicylaldehyde (Sal) as a secondary ligand to produce $[La(L)Cl_2(NH_3)]$, [La(L)Cl(Fur)], or [La(L)Cl(Sal)] (2-5) complexes respectively after stirred and refluxed for 6 hours.

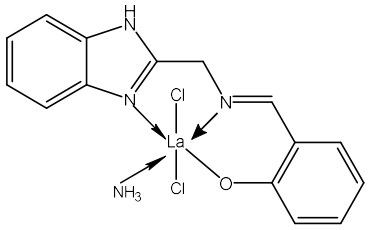

Structure of Benzimidazole Schiff Base $[La(L)Cl_2(NH_3)]$ Complex (3)

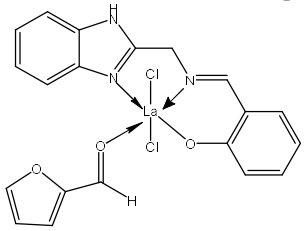

Structure of Benzimidazole Schiff Base [La (L) Cl (Fur)] Complex (4)

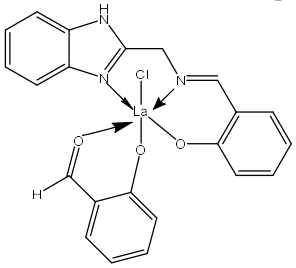

Structure of Benzimidazole Schiff Base [La(L)Cl (Sal)] Complex (5)

3.2.2.1 Benzimidazole Schiff Base $[La(L)Cl_2(NH_3)]$ Complex (3)

Pale orange color. Yield: 72.5%. Data of the elemental analysis for the complex for $C_{15}H_{15}N_4OCl_2La$ (FW= 477.12) calculated: C, 37.76%; H, 3.17%; N, 11.74% found: C, 37.4 %; H, 3.2%; N, 11.7%. FT-IR (KBr, disc cm^{-1}, υ_{max}/ cm^{-1}) for the complex, 3335, 3208 (N-H/ NH_3), 3053-2582 (NH…O), 2127 (C-O) phenyl, 1623 (C=N) azomethine, 1615 (C=N) ring, 726 (La←N), 684 (La-O), and 439 (La-Cl). ^{1}HNMR (ppm DMSO-d_6): δ 8.43 (s, 1H, CH=N), 7.18–7.40 (m, 8 Ar H), δ 4.13 (s, 2H, CH_2-N). ^{13}C NMR (ppm *d*6-

DMSO): δ 115.76–143.11 (Ar carbons), 164.12 (HC=N), 160.41 (C-O), 60.42 (CH_2) [36].

3.2.2.2 Benzimidazole Schiff Base [La(L)Cl (Fur)] Complex (4)

Yellow color. Yield: 67.7%. Data of the elemental analysis for $C_{20}H_{16}N_3O_3Cl_2La$ (FW= 556.17) calculated: H, 2.90%; C, 43.19%; N, 7.56% found: H, 2.87%; C, 43.12 %; N, 7.53%. FT-IR (KBr, disc cm^{-1}, υ_{max}/ cm^{-1}) for the complex, 3260 (N-H), 3140-2600 (NH…O), 2123 (C-O) phenyl, 1710 (C=O), 1618 (C=N) azomethine, 1605 (C=N) ring, 734 (La←N), 687 (La-O), and 428 (La-Cl). ^{1}HNMR (ppm DMSO-d_6): *δ* 9.72 (s, 1H, aldehydic proton) *δ* 8.34 (s, 1H, CH=N), 7.19–7.52 (m, 8 ArH), *δ* 7.58-8.2 (m, 3H furan ring)), δ 4.23 (s, 2H, CH2-N). ^{13}C NMR (ppm *d*6-DMSO): δ 110.5–156.46 (Ar carbons), 162.00 (HC=N), 160.63 (C-O), 61.23 (CH_2), and 178.92 (C=O) [37].

3.2.2.3 Benzimidazole Schiff Base [La(L)Cl(Sal)] Complex (5)

Orange color. Yield: 70.2%. Data of the elemental analysis for the complex $C_{22}H_{17}N_3O_3ClLa$ (FW= 545.75) calculated: H, 3.14%; C, 48.42%; N, 7.70% found: H, 3.11%; C, 48.21 %; N, 7.66%. FT-IR (KBr, disc cm^{-1}, υ_{max}/ cm^{-1}) of the complex, 3450 (H_2O), 3258 (N-H), 2120 (C-O) phenyl, 1730 (C=O), 1609 (C=N) azomethine, 1600 (C=N) ring, 739 (La←N), 662 (La-O), and 416 (La-Cl). ^{1}HNMR (ppm DMSO-d_6): *δ* 10.3 (s, 1H, aldehydic proton) *δ* 8.30 (s, 1H, CH=N), 7.0–7.6 (m, 12 ArH), δ 4.15 (s, 2H, CH_2-N). ^{13}C NMR (ppm *d*6-DMSO): δ 115.74–155.24 (Ar carbons), 163.64 (HC=N), 160.51 (C-O), 60.89 (CH_2), and 191.44 (C=O) [38].

4. Results and discussion

4.1 Molar Conductivity

The complexes' molar conductivity gave low values (11- 23) Ω^{-1} cm^2 mol^{-1}, indicating that the formed complexes with lanthanum metal is non-ionic compounds.

4.2. Spectroscopy

As of the difficulty of dissolving the ligand in ethanol, we used DMF solvent to dissolve it and study it. In the ligand, there were lone pairs of electrons and π electrons in the ligand. Therefore, three different transitions at absorbance values of the ligand showed at 273 nm indicating the π→π* transition, the transition reported at 319 nm, indicating the transition in the n → π * band, the highest transition reported at 422 nm, which corresponds to (2) 3A2 g (F) → 3T1g (F), respectively.

The UV-Visible spectrum of the formed complexes' showed electronic charge transfer only. This is because the d orbital had no electrons. Moreover, electronic transitions of the π→π* and n→π* types, which were originally present in the ligand, appeared. Mixed ligands complexes (2-5) showed slightly various colors because the lanthanum ion had no electron in the d orbital. The reason of the appearance of these colors in the complexes is the electronic transition n→π*, π→π*and the ligand to metal charge transfer (LMCT) [39].

4.3. IR spectra

Infrared spectra of synthesized metal complex are shown in Figure1. Ligand **(1)** infrared spectrum showed absorption bands in the 3450 and 3300 cm^{-1} regions indicating the free phenolic hydroxyl group and the (NH) group on the benzimidazole ring. Five main bands in

the 3290-3300 cm^{-1} range showed the IR spectrum in the N-H stretching vibrations in the complexes. The absorption band of azomethine group (-N=C-) was at 1610 cm^{-1}; while the ligand showed an absorption band in the1590 and 1550 cm^{-1} denoting υ(N=C) and υ(-C=C-) in the ring [38].

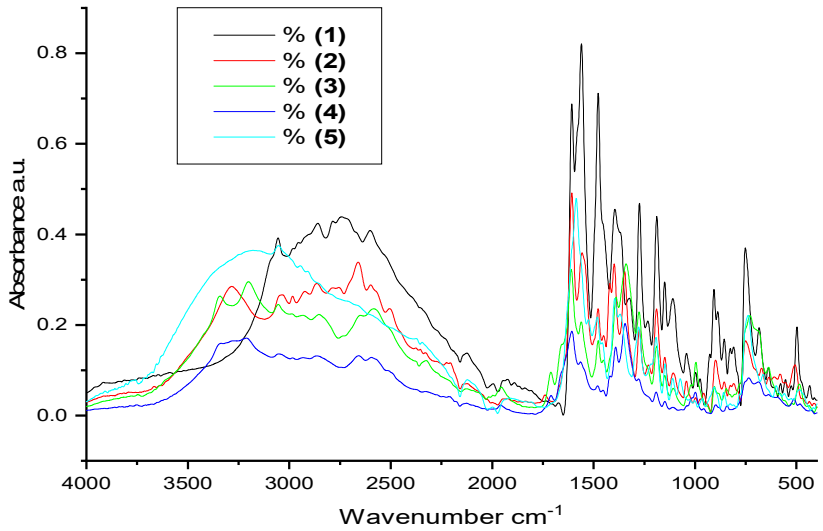

Figure 1. Infrared spectra of synthesized metal complex

The ligand serves as a tridentate ionic compound, bound with lanthanum (III) via the nitrogen atom of benzimidazole Penta ring, the nitrogen atom of the azomethine group, and the oxygen atom of the hexagonal phenolic ring. The **complex (2)** infrared spectra exhibited a vibration region in 3450 - 3330 cm^{-1} range, coordinated water molecule with a lanthanum ion was suggested. Another vibration band that appeared in the 3300 cm^{-1} region indicated that the NH group oscillation in the five-pointed ring of the benzimidazole compound. The band characteristic to υ (NH) was still present in a similar position indicating that this group did not participate in the coordination. Shift frequencies appeared to lower values at 1600 and 1580 cm^{-1} indicated to coordination azomethine group and (C=N) with the metal ion. The complex also showed absorption bands in the regions 750 cm-1 and 620 cm^{-1} correspondingly to the binding of oxygen υ (O-M) and nitrogen υ (N-M) to the lanthanum ion. The complex also showed an absorption band at a value of 390 cm^{-1}, indicating the bonding of the chlorine ion with the lanthanum ion [40].

Complex (3) showed an absorption double band in the region of 3320 cm^{-1}, 3280 cm^{-1}, and the disappearance of the broad absorption band of water in the main complex indicates the substitution of the ammonia molecule instead of the water molecule that was bound with the lanthanum ion. This process indicates the formation of a mixture of ligands bound with a metal ion. The remaining groups' absorption bands associated with the lanthanum ion showed a slight shift towards the lower frequency and by the amount of 5 cm^{-1} for the azomethine group and 4 cm^{-1} for the deprotonated hydroxyl group while the group (C=N) remained at the same previous absorption bands. As mentioned earlier, the complex also showed an absorption band at a value of 390 cm^{-1}, indicating the bonding of the chlorine ion with the lanthanum ion.

The IR spectrum of **complex (4)** showed the Schiff base ligand band at 1600 cm^{-1} of azomethine indicated to ν(C=N) with the metal ion. The ν (OH) (phenolic group) at ligand (1) is not found in the compound (4) spectrum, suggesting coordination of to the metal ion via the deprotonated phenolic oxygen. This is also confirmed with the absorption band shift of ν(C–O) to a higher frequency band via 20 cm^{-1} compared to ν(C–O) (phenolic) at 1537 cm^{-1} in the free ligand. A medium-strong band appearing at 1100 cm^{-1} in the complex corresponds to the bonded hydroxo groups' vibrations. Furfural molecule showed a frequency band at 1650 cm^{-1}, indicating a bond with metal ion through (C=O) group this value. It is a low value compared with the frequency band of the free group in the furfural aldehyde molecule, indicating its bonding.

Complex (5) the band showed at 1605 cm^{-1} the Schiff base ligand of azomethine indicated to ν(C= N) with the metal ion. Also, the ν(OH) (phenolic group) at ligand **(1)** is not found in the spectrum of complex (5), suggesting deprotonated phenolic oxygen coordination of to the metal ion. This is also confirmed by the absorption band of ν(C–O) at 1540 cm^{-1} with a 20cm^{-1} higher frequency shift comparing with ν(C–O) (phenolic) in the free ligand. The medium-strong band that appeared at 1105 cm^{-1} in the complex refers to the bonded hydroxo group's vibrations. Salicylaldehyde aldehyde molecule showed a frequency band at 1660 cm^{-1}, indicating a bond with metal ion through (C=O) group this value is low compared to the free group's frequency band in the furfural aldehyde molecule, indicating its bonding.

4.4. Thermal analysis

The thermal analyzes of the prepared complexes showed an agreement with the findings of the other analyzes and the characterization of the chemical compounds. Therefore, the TG and DTG curves of the mixed ligands complexes were shown that the metal complexes decompose in three steps. **Complex (2)** showed the first step of a decomposition range from 120–140°C, with 3.79% weight loss, which refers to the one molecule of water deficiency (calcd. 3.75%) found (3.70%). The reality that the loss of one water molecule at a high temperature proposes the coordination of water. The second losing point showed losing of weight between 280- 300°C, with a weight loss of (calcd. 15.43%) found (15.50%), which matches of the loss of one chloride molecule [41]. The third point showed a continuous weight loss at range temperature 350 and 550°C. The complex is finally converted to the oxide by weight ratio (calcd. 83.54% found 83.23%), La2O3 is the final product.

Complex (3) represented the losing weight loss point has a decomposition range of 220–260°C, with a weight loss (Calcd. 3.56%, corresponding to ammonia molecule losing (Found. 3.60%). The ammonia molecule was lost at a higher temperature proposes the strong bond of a coordinated group with the metal ion. A continuous weight losing between 280- 290°C, with a weight loss of (calcd. 15.43%) found (15.50%), which matches the loss of one chloride molecule [42-47]. The third point showed a continuous weight loss at range temperature 370 and 550°C. The complex is finally converted to the oxide by weight ratio (calcd. 83.54% found 83.23%), La2O3 is the final product.

Complex (4) showed the weight loss at a temperature of 250°C, with a weight loss of (Calcd. 17.26%, corresponding to the loss of furfural aldehyde (Found. 17.50%). The reason for the exit of the furfural aldehyde molecule before the chlorine molecule was its large size

and formation, steric effects around the lanthanum ion. The second losing weight point showed weight loss between 270°C and 285°C, with a weight loss of (calcd. 15.43%) found (15.50%), which matches of the loss of one chloride molecule. The third point showed a continuous weight loss at range temperature 400 and 550°C. The complex is finally converted to the oxide by weight ratio (calcd. 83.54% found 83.23%), La_2O_3 is the final product.

Complex (5) this complex showed a different change in the exit sequence of its component groups. In the first step, the chloride ion begins to exit due to the bond's strength that binds the Salicylaldehyde with the lanthanum (III) ion. The complex showed at a temperature range of (284-292 °C) with a weight loss of about (Calcd. 6.51%) corresponding to the loss of chloride ion (Found. 6.61%). The second weight-loss point showed a continuous weight loss between 380°C, with a weight loss of (calcd. 23.72%) found (23.50%), which matches the loss of one Salicylaldehyde molecule. The third point showed a continuous weight loss at a temperature of 550°C. The complex is finally converted to the oxide by weight ratio (calcd. 83.54% found 83.23%), La_2O_3 is the final product.

4.5. XRD spectrometry

The XRD patterns for the four complexes were illustrated in Table 1 and Figure 2. Using some software. The XRD measurements output data were refined and analyzed. XRD There are many programming codes that can be used for the analysis X-ray line profile. The used software in this study is residual peak fitting (Peak Fit), to help identify, isolate, measure the hidden peaks that are missed by normal instrumentation, and accurate background. Also Peak Fit involves various nonlinear line forms for the spectral application [48-50].

Table 1. X-ray powder diffraction crystal parameters of complexes (2- 4): Lattice constant, inter axial angle, crystal system, space group, unit cell volume, and crystallite size.

Parameters		Complex (2)	Complex(3)	Complex(4)	Complex(5)
Empirical formula		$C_{15}H_{14}O_2N_3Cl_2La$	$C_{15}H_{14}ON_4Cl_2La$	-	$C_{22}H_{17}O_3N_3ClLa$
Lattice constant	a (Å)	8.566	8.477	-	8.476
	b (Å)	14.006	12.052	-	12.265
	c (Å)	14.822	13.765	-	12.895
Interaxial angle	**α (°)**	90.55	90.05	-	90.22
	β (°)	114.67	116.15	-	116.18
	γ (°)	90.11	90.19	-	91.13
Crystal system		a≠b≠c, α ≠β ≠γ	a≠b≠c, α ≠β ≠γ		a≠b≠c, α ≠β ≠γ
		Triclinic	Triclinic	-	Triclinic
Space group		$P\bar{1}$	$P\bar{1}$	-	$P\bar{1}$
Unit cell Volume (Å^3)		1615.23	1262.22	-	1185.89
Crystal Size		68.80	59.70	Amorphous	40.56

For the four complexes, a standard cell parameter was used as starting values for the program "CHEKCELL" to classify the Bragg reflections [48-49]. The program of CHEKCELL is powder indexing software. The parameters of the crystal lattice were calculated with its aid [48-49].

The crystal data of the four complexes were analyzed, and the triclinic crystal system is well fitted for all complexes except complex number (4) which is amorphous and gave a broad XRD band. Table 1 describes the unit cell parameters of the crystalline complexes. The different values for the measured volumes of unit cells result from impurities sizes inserted into the main material. Also, the large atom/molecule size would cause increasing the cell unit volume, resulting in bond deformation as well as changes in the components of the material of the product.

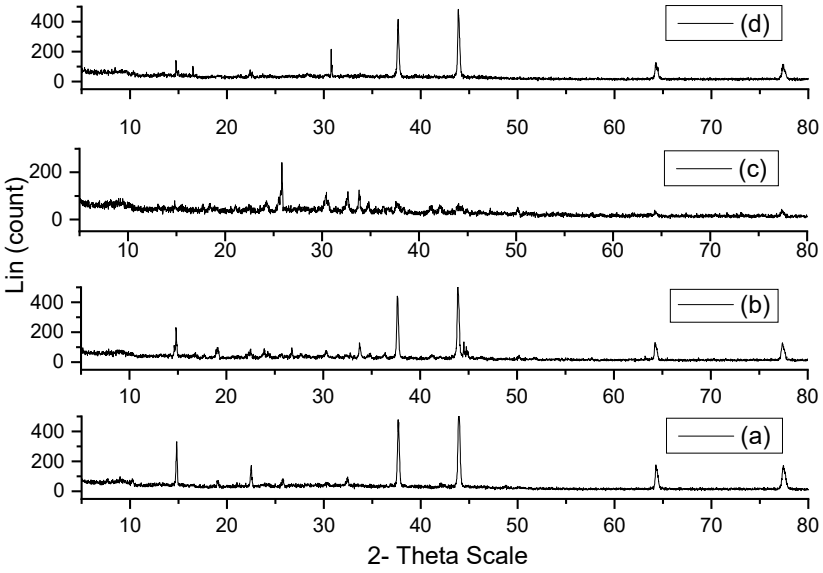

Figure 2. XRD pattern of (a) Complex 2, (b) Complex 3, (c) Complex 4, and (d) Complex 5

Furthermore, using the average crystallite sizes of the complexes, the diffraction data, and D, which has been determined using the Scherer equation: ($D = 0.9\lambda/(\beta\cos\theta)$, where θ symbol is Bragg diffraction angle, λ symbol is X-ray wavelength (1.54180 Å), and β symbol is the strong diffraction peak full width at half maximum of the samples [48]. But for broaden peak such as in Complex **(2)**, the Peak fit program identified the most intensity without broadening, so the crystallite size was calculated using the Scherer equation after deconvolution of the X-ray line profile. Fig. 2 represented that **(2-5)** complexes high crystallinity, also the XRD patterns indicate the presence of the complexes in nano size. Whereas complex **(2)** exhibited broadening that proves the deformation of binding in this

complex. The average size of the four complexes was computed and represented in Table 1, these values indicate that complex **(2)** is more crystalline than the other complexes.

4.6. Antibacterial and Antifungal Screening

The mixed ligands complexes were screened for their antibacterial and antifungal activities and the results obtained are presented in Table 2 and Figure 3. It is observed that the activity of the mixed ligand complexes changes with a change in the secondary ligand. This type of behavior is explained considering Tweedy's chelation theory and Overtone's concept [49, 50]. The mixed ligand complexes are more potent bactericides than the free parental ligand. The activities against G (–) *Escherichia coli* were in the order complex (4) [La (L) Cl(Fur)] > complex (2) [La (L) $Cl_2(H_2O_2)$] and complex (3) [La(L)$Cl_2(NH_3)$]> complex (5) [La (L)Cl(Sal)]> Ligand (HL) (1). The complex activities against G (+) *Staphylococcus aureus* were in the order complex(2) [La(L)$Cl_2(H_2O_2)$] and complex (4) [La(L)Cl(Fur)] > and complex (3) [La(L)Cl2(NH3)] and complex (5) [La(L)Cl(Sal)] > Ligand (HL) (1). The metal complexes also have fungicide effect against *Candida albicans* in the order complex (2) [La (L) $Cl_2(H_2O_2)$] and Ligand (HL) (1) > complex (4) [La(L)Cl(Fur)] > complex (3) [La(L)$Cl_2(NH_3)$] > complex (5) [La(L)Cl(Sal)]. There was no fungicide activity against *Aspergillus flavus*, this may be due to their cell membrane morphology [51].

Table 2. Antibacterial and antifungal activities of complexes by the diameter of the growth inhibition zone (mm / mg sample).

Sample		Inhibition zone diameter (mm / mg sample)			
		Bacterial species		Fungal species	
		Escherichia coli (G^-)	*Staphylococcus aureus* (G^+)	*Aspergillus flavus*	*Candida albicans*
Control : DMSO		0.0	0.0	0.0	0.0
Standard	Ampicillin Antibacterial agent	25	21	--	--
	Amphotericin B Antifungal agent	--	--	17	21
(HL) (1)		11	14	0.0	13
Complex (2)		14	16	0.0	13
Complex (3)		14	15	0.0	9
Complex (4)		16	16	0.0	12
Complex (5)		12	15	0.0	10

The complexes activities in **Table 2** disclosure that the behavior of the complexes is impaired by the existence of the substituent(s) and donor site of the ligands, in relation to their membrane permeability, a crucial factor in allowing their entrance into the cell [52, 56].

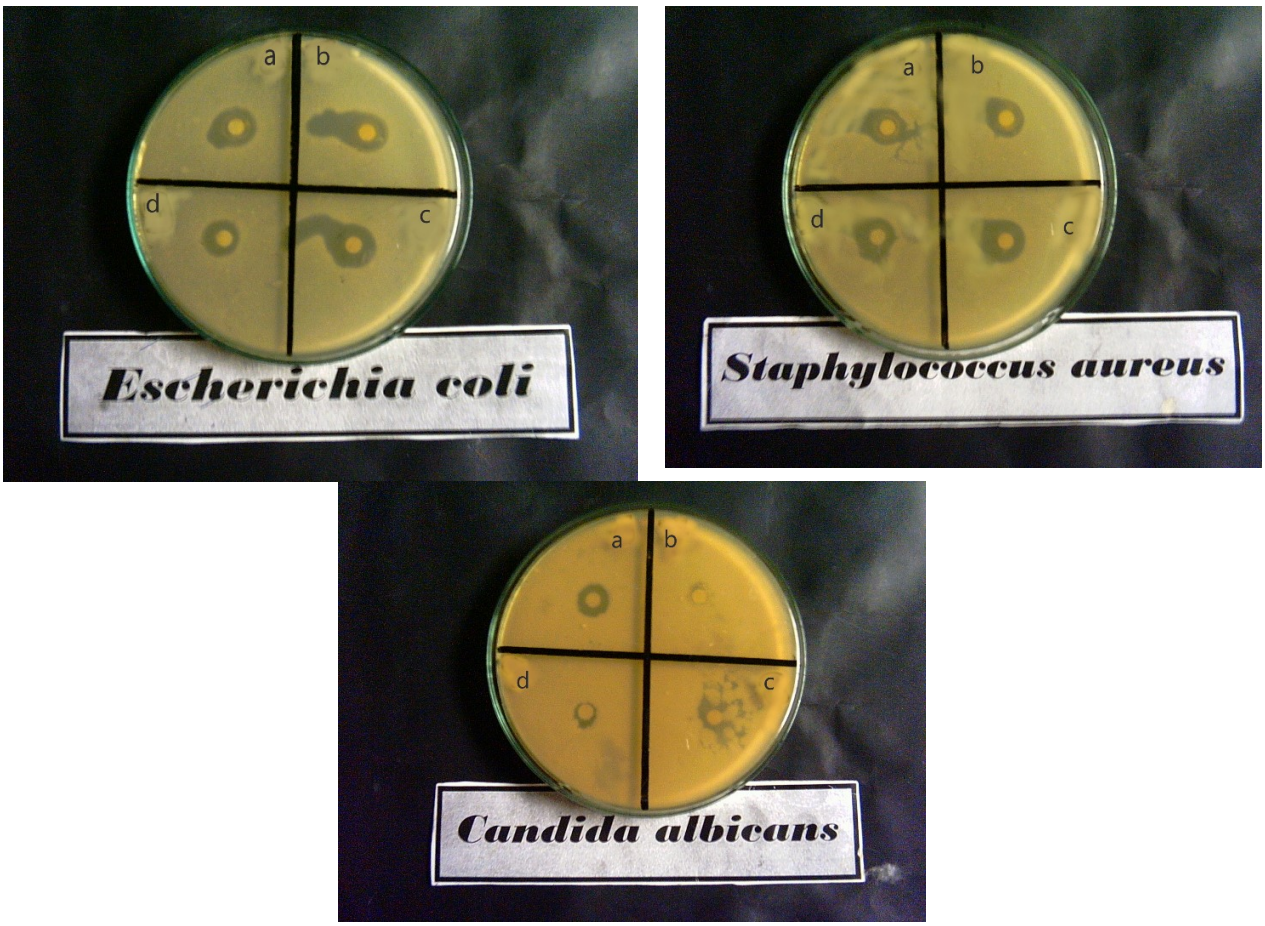

Figure 3. Images of antimicrobial and antifungal activities for complexes (a) Complex **(2)** (b) Complex **(3),** (c) Complex **(4)**, and (d) Complex **(5)** against *Escherichia coli*, *Staphylococcus aureus*, and *Candida albicans.*

4.7. Anticancer activity:

The *in vitro* cytotoxic behavior of the compounds were calculated by using Sulphorhodamine-B (SRB) assay as described in the experimental part towards colon HCT116 and liver HEPG2 tumor cell lines with a concentration range from 0 to 100 µg/ml as described in the methodology section. The results in Figures **4 and 5** show the relationship between cell survival fraction of human tumor carcinoma cell lines and drug concentration.

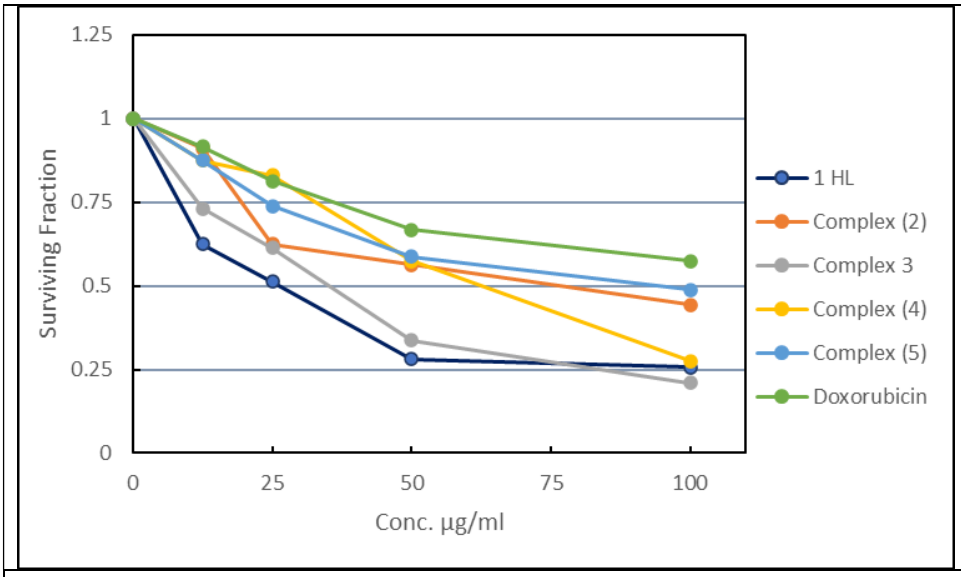

Figure 4. Cytotoxic effect of complexes on the HCT116 cell line

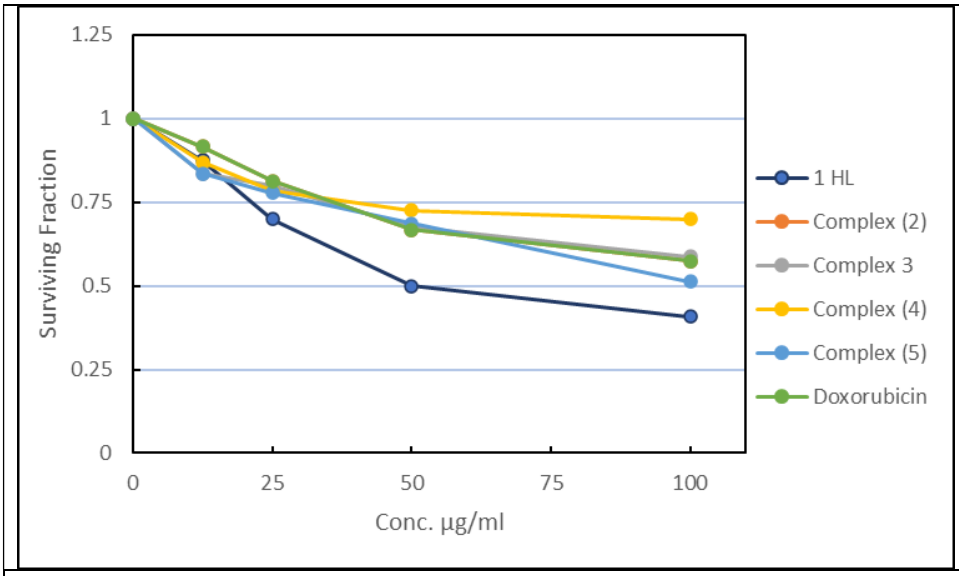

Figure 5. Cytotoxic effect of complexes on the HEPG2 cell line

Figure 4 shows the HCT116 cell line cytotoxicity; Compound (1) (HL) showed IC_{50} at 27 µg/ml, complex (3) [La (L) $Cl_2(NH_3)$] showed IC_{50} at 34.6 µg/ml, Complex (4) [La(L)Cl(Fur)] showed IC_{50} at 63 µg/ml, complex (2) [La (L) $Cl_2(H_2O_2)$]showed IC_{50} at 75 µg/ml, and complex (5) [La (L) Cl(Sal)] showed the lowest HCT116 cell line cytotoxicity at 92 µg/ml.

As shown in **Figure 5**, tested drugs complexes showed variable cytotoxic activity against HEPG2 tumor human cell line; Compound 1 (HL) and complex (5) [La(L)Cl(Sal)] showed IC_{50} near 50 µg/ml near while the complex (3) [La (L) $Cl_2(NH_3)$] and complex (2) exhibit IC_{50} near 100 µg/ml. However, the complex (4) [La (L) Cl (Fur)] showed very

weak cytotoxicity. In general, each drug was lower in the case of HEPG2 cell line than in HCT116 cell line. From the above, we can say that the mixed ligand complex (3) [La (L) Cl_2 (NH_3)] of lanthanum ammonia showed the highest efficacy against HCT116 cell line with a low concentration in comparison with the other ligands. There is a previous report showing that this complex reduced the cell proliferation and increased the apoptosis in the HCT116 cancer cell [57].

5. Conclusion

The complexes formed from the mixture of ligands have unique and varied properties since they contain different ligands. In our research, we prepared a mixture of ligands with lanthanum (III). The prepared mixture of ligands showed an apparent effect on some types of gram-negative and gram-positive bacteria, as well as on types of fungi arranged according to their effectiveness as follows:

The activities against G (–) *Escherichia coli* were in the order complex (4) > complex (2) complex (3) > complex (5) > (HL) (1). The complex activities against G (+) *Staphylococcus aureus* were in the order complex (2) and complex (4) > and complex (3) and complex (5) > Ligand (HL) (1). The metal complexes also have fungicide effect against *Candida albicans* in the order complex (2) and (HL) (1) > complex (4) > complex (3) > complex (5).

In our study, we analyzed the effect of the prepared ligand complexes in HCT116 colon and HEPG2 liver cancer cell lines with a concentration range of 0 to 100 μg / ml. The ligand and the complexes showed impressive results characterized by their high effectiveness against cancer cells when compared to some drugs used as anti-cancer therapy with the method of Sulphorhodamine-B (SRB). The mixed ligands complex shows the HCT116 cell line cytotoxicity; Compound (1) (HL) showed IC_{50} at 27 μg/ml, Complex (3) showed IC_{50} at 34.6 μg/ml, Complex (4) showed IC_{50} at 63 μg/ml, Complex (2) showed IC_{50} at 75 μg/ml, and complex (5) showed the least HCT116 cell line cytotoxicity at 92 μg/ml. Tested drugs complexes showed variable cytotoxic activity against HEPG2 tumor human cell line; Compound 1 (HL) and complex (5) showed IC_{50} near 50 μg/ml near while the complex (3) and complex (2) exhibited IC_{50} near 100 μg/ml. Complex (4) showed very weak cytotoxicity.

6. References

1. Singh, P.K. and O. Silakari, *The Current Status of O-Heterocycles: A Synthetic and Medicinal Overview.* ChemMedChem, 2018. **13**(11): p. 1071-1087.
2. Pathania, S. and P.A. Chawla, *Thiophene-based derivatives as anticancer agents: An overview on decade's work.* Bioorganic Chemistry, 2020: p. 104026.
3. El-Molla, M.M., S.A. Shama, and S. El-Sayed Saeed, *Preparation of disappearing inks and studying the fading time on different paper surfaces.* Journal of forensic sciences, 2013. **58**(1): p. 188-194.
4. Shama, S., et al., *Fading time study on prepared thymolphthalein, phenolphthalein and their mixture disappearing ink.* Research Journal of Textile and Apparel, 2008. **12**(1): p. 9.

5. Abdel-Rahman, A., et al., *Synthesis and biological activity of some new benzimidazolyl-azetidin-2-ones and-thiazolidin-4-ones.* Die Pharmazie, 1983. **38**(9): p. 589-590.
6. Yadav, S., et al., *Synthesis and evaluation of antimicrobial, antitubercular and anticancer activities of benzimidazole derivatives.* Egyptian Journal of Basic and Applied Sciences, 2018. **5**(1): p. 100-109.
7. Akhtar, M.J., et al., *Recent progress of Benzimidazole hybrids for anticancer potential.* Current Medicinal Chemistry, 2020.
8. Habernickel, V., *Alkyl-5-heterocyclic-benzimidazolyl-carbamate Derivatives.* Drugs made in Germany, 1992. **35**: p. 97.
9. Karaburun, A.Ç., et al., *Synthesis and antifungal potential of some novel benzimidazole-1, 3, 4-oxadiazole compounds.* Molecules, 2019. **24**(1): p. 191.
10. Eswayah, A., et al., *Evaluation of Antioxidant, Analgesic and Anti-inflammatory Activity of 2-(4-Aminophenyl) Benzimidazole-based Schiff Bases.*
11. Francesconi, V., et al., *Synthesis and Biological Evaluation of Novel (thio) semicarbazone-Based Benzimidazoles as Antiviral Agents against Human Respiratory Viruses.* Molecules, 2020. **25**(7): p. 1487.
12. AL-FAKEH, M.S., et al., *Synthesis and Properties of Two Fe(III) Coordination Polymers Based on 2-Amino-4-methylthiazole, 2-Mercaptobenzothiazole and Aromatic Polycarboxylate.* Asian Journal of Chemistry, 2020. **32**(10): p. 2502-2506.
13. Al-Hakimi, A.N., et al., *Design, synthesis, characterization of zirconium (IV), cadmium (II) and iron (III) complexes derived from Schiff base 2-aminomethylbenzimidazole, 2-hydroxynaphtadehyde and evaluation of their biological activity.* Arabian Journal of Chemistry, 2020. **13**(10): p. 7378-7389.
14. Schiff, H., *Mittheilungen aus dem Universitätslaboratorium in Pisa: eine neue Reihe organischer Basen.* Justus Liebigs Annalen der Chemie, 1864. **131**(1): p. 118-119.
15. Cordeiro, R. and M. Kachroo, *Synthesis and biological evaluation of anti-tubercular activity of Schiff bases of 2-Amino thiazoles.* Bioorganic & Medicinal Chemistry Letters, 2020. **30**(24): p. 127655.
16. Patil, P., et al. *Synthesis, characterisation and biological investigation of some third-row elements with halo-substituted coumarin schiff base with N and O as donors*. in *IOP Conference Series: Materials Science and Engineering*. 2020. IOP Publishing.
17. Al-Hakimi, A.N., et al., *Synthesis, Spectroscopic Characterization and Antimicrobial Activity of Novel Azo-acetohydrazide Metal Complexes.* Journal of Natural Sciences and Mathematics, 2017. **10**(1).
18. Ahamad, M.N., et al., *Anticancer properties, apoptosis and catecholase mimic activities of dinuclear cobalt (II) and copper (II) Schiff base complexes.* Bioorganic Chemistry, 2020. **95**: p. 103561.

19. Uzzaman, M., M. Junaid, and M.N. Uddin, *Evaluation of anti-tuberculosis activity of some oxotitanium (IV) Schiff base complexes; molecular docking, dynamics simulation and ADMET studies.* SN Applied Sciences, 2020. **2**(5): p. 1-11.
20. Kareem, M.J., et al., *Synthesis, characterization, and determination antioxidant activities for new Schiff base complexes derived from 2-(1H-indol-3-yl)-ethylamine and metal ion complexes.* Journal of Molecular Structure, 2020: p. 129669.
21. Sakhare, D., *Synthesis, Characterization of Schiff Bases and Biological Activities of Their Transition Metal Complexes-Review.* International Journal of Advanced Science and Engineering, 2020. **6**(04): p. 1538-1544.
22. Farouk, A., et al., *Photocatalytic activity and antibacterial properties of linen fabric using reduced graphene oxide/silver nanocomposite.* RSC Advances, 2020. **10**(68): p. 41600-41611.
23. Saeed, M.M.A.E.-H. and S. El-Sayed, *Antibacterial Properties and pH Sensitive Swelling of Insitu Formed Silver-Curcumin Nanocomposite Based Chitosan Hydrogel*. 2020, MDPI.
24. Saeed, S.E.-S., et al., *Novel chitosan-ZnO based nanocomposites as luminescent tags for cellulosic materials.* Carbohydrate polymers, 2014. **99**: p. 817-824.
25. Saeed, S., M. Abdel-Mottaleb, and M. Abdel-Mottaleb, *One-Step thermolysis synthesis of divalent transition metal ions monodoped and tridoped CdS and ZnS luminescent nanomaterials.* Journal of Nanomaterials, 2014. **2014**.
26. Sharaf, S., A. Farouk, and M. El-Hady, *Novel conductive textile fabric based on polyaniline and CuO nanoparticles.* Int J PharmTech Res, 2016. **9**(6): p. 461À72.
27. Vogel, A.I. and G.H. Jeffery, *Vogel's textbook of quantitative chemical analysis*. 1989: Wiley.
28. Bauer, A.W., et al., *Antibiotic Susceptibility Testing by a Standardized Single Disk Method.* American Journal of Clinical Pathology, 1966. **45**(4_ts): p. 493-496.
29. Chang, J.-C., et al., *Antimicrobial susceptibility of flavobacteria as determined by agar dilution and disk diffusion methods.* Antimicrobial agents and chemotherapy, 1997. **41**(6): p. 1301-1306.
30. Matar, M.J., et al., *Correlation between E-test, disk diffusion, and microdilution methods for antifungal susceptibility testing of fluconazole and voriconazole.* Antimicrobial agents and chemotherapy, 2003. **47**(5): p. 1647-1651.
31. Skehan, P., et al., *New colorimetric cytotoxicity assay for anticancer-drug screening.* JNCI: Journal of the National Cancer Institute, 1990. **82**(13): p. 1107-1112.
32. Vichai, V. and K. Kirtikara, *Sulforhodamine B colorimetric assay for cytotoxicity screening.* Nature protocols, 2006. **1**(3): p. 1112-1116.
33. Song, W.-J., et al., *Synthesis, interaction with DNA and antiproliferative activities of two novel Cu (II) complexes with Schiff base of benzimidazole.* Spectrochimica Acta Part A: Molecular and Biomolecular Spectroscopy, 2014. **121**: p. 70-76.
34. Shakdofa, M.M., et al., *Transition metal complexes of a hydrazone–oxime ligand containing the isonicotinoyl moiety: Synthesis, characterization and microbicide activities.* Applied Organometallic Chemistry, 2018. **32**(7): p. e4376.

35. Wahba, M.A., et al., *Preparation, Characterization and Antimicrobial Activities of N'-((3-(hydroxyimino) butan-2-ylidene)-2 (phenylamino) acetohydrazide and Its Metal Complexes.* Egyptian Journal of Chemistry, 2017. **60**(1): p. 1-24.
36. El-Saied, F.A., et al., *Antitumor activity of synthesized and characterized Cu (II), Ni (II) and Co (II) complexes of hydrazone-oxime ligands derived from 3-(hydroxyimino) butan-2-one.* Beni-Suef University journal of basic and applied sciences, 2018. **7**(4): p. 420-429.
37. Shakdofa, M.M., et al., *Synthesis, characterization and bioactivity¬¬¬¬ Zn2+, Cu2+, Ni2+, Co2+, Mn2+, Fe3+, Ru3+, VO2+ and UO22+ complexes of 2-hydroxy-5-((4-nitrophenyl) diazenyl) benzylidene)-2-(p-tolyl-amino) acetohydrazide.* Bulletin of the Chemical Society of Ethiopia, 2017. **31**(1): p. 75-91.
38. El-Saied, F.A., et al., *Anti-neurotoxic evaluation of synthetic and characterized metal complexes of thiosemicarbazone derivatives.* Applied Organometallic Chemistry, 2018. **32**(4): p. e4215.
39. El-Tabl, A.S., et al., *Synthesis, Characterization and Biological Studies of New Mn (II), Ni (II), Co (II), Cu (II) and Zn (II) of 2-(benzothiazol-2-yl)-N'-(2, 5-dihydroxybenzylidene) acetohydrazide.* Journal of the Korean Chemical Society, 2011. **55**(1): p. 19-27.
40. El-Tabl, A.S., et al., *Antimicrobial activities of the metal complexes of N'-(5-(4-chlorophenyl) diazenyl)-2-hydroxybenzylidene)-2-hydroxybenzohydrazide.* Main Group Chemistry, 2012. **11**(4): p. 311-327.
41. El-saied, F.A., et al., *Transition metal complexes derived from N'-(4-fluorobenzylidene)-2-(quinolin-2-yloxy) acetohydrazide: Synthesis, structural characterization, and biocidal evaluation.* Applied Organometallic Chemistry, 2020. **34**(11): p. e5898.
42. Shakdofa, M.M., F.A. El-Saied, and A.N. Al-Hakimi, *Synthesis, spectroscopic characterization and biological activity of 2-(p-toluidino)-N'-(2-hydroxbenzylidene) acetohydrazide complexes.* Main Group Chemistry, 2012. **11**(3): p. 189-204.
43. Alminderej, F.M., *Synthesis, Design and Biological Evaluation of Antibacterial Activity of Novel Mixed Metal Complexes Derived from Benzoimidazolphenylethanamine and 6-Amino-N, N-dimethyluracil.* Letters in Organic Chemistry, 2021. **18**(2): p. 95-106.
44. Alhakimi, A.N., *Synthesis, Characterization and Microbicides Activities of N-(hydroxy-4-((4-nitrophenyl) diazenyl) benzylidene)-2-(phenylamino) Acetohydrazide Metal Complexes.* Egyptian Journal of Chemistry, 2020. **63**(4): p. 1509-1525.
45. Shakdofa, M.M., et al., *Synthesis, characterization, and density functional theory studies of hydrazone–oxime ligand derived from 2, 4, 6-trichlorophenyl hydrazine and its metal complexes searching for new antimicrobial drugs.* Applied Organometallic Chemistry, 2021. **35**(2): p. e6111.
46. Alorini, T.A., et al., S*ynthesis, characterization, and anticancer activity of some metal complexes with a new Schiff base ligand. Arabian Journal of Chemistry*, 2022. **15**(2): p. 103559.

47. Alhakimi, A.N., et al., *Transition Metal Complexes Derived From 2-hydroxy-4-(p-tolyldiazenyl) benzylidene)-2-(p-tolylamino) acetohydrazide Synthesis, Structural Characterization, and Biological Activities.* Journal of the Korean Chemical Society, 2021. **65**(2): p. 93-105.
48. Laugier, J. and B. Bochu, *Chekcell: Graphical powder indexing cell and space group assignment software*. 2004.
49. Miranda, M. and J. Sasaki, *The limit of application of the Scherrer equation.* Acta Crystallographica Section A: Foundations and Advances, 2018. **74**(1): p. 54-65.
50. Mallah, A., *Structural, magnetic and magnetocaloric properties of nickel-copper ferrite with chromium substitution.* Journal of Natural Sciences and Mathematics, 2018. **11**(1).
51. Al-Hakimi, A.N., et al., *N, N 2-bis (3-((3-hydroxynaphthalen-2-yl) methylene-amino) propyl) phthalamide 의크롬 (III), 망간 (II), 철 (III), 코발트 (II), 니켈 (II), 구리 (II), 루테늄 (III) 및 산화 지르코늄 (II) 착물에 대한 합성과 분광학 및 생물학적 연구.* Journal of the Korean Chemical Society, 2011. **55**(3).
52. Login, C.C., et al., *A Novel Thiazolyl Schiff Base: Antibacterial and Antifungal Effects and In Vitro Oxidative Stress Modulation on Human Endothelial Cells.* Oxidative medicine and cellular longevity, 2019. **2019**.
53. El-Hady, A., et al., *Multiwalled-Carbon-Nanotubes (MWCNTs)–GPTMS/Tannic-Acid-Nanocomposite-Coated Cotton Fabric for Sustainable Antibacterial Properties and Electrical Conductivity.* Coatings, 2022. **12**(2): p. 178.
54. Shakdofa, M.M., et al., *Synthesis, characterization and bioactivity [Zn. sup. 2+],[Cu. sup. 2+],[Ni. sup. 2+],[Co. sup. 2+],[Mn. sup. 2+],[Fe. sup. 3+],[Ru. sup. 3+], V [O. sup. 2+] and U [O. sub. 2. sup. 2+] complexes of 2-hydroxy-5-((4-nitrophenyl) diazenyl) benzylidene)-2-(p-tolylamino) acetohydrazide.* Bulletin of the Chemical Society of Ethiopia, 2017. **31**(1): p. 75-92.
55. Aramesh-Boroujeni, Z., et al., *Experimental and computational interaction studies of terbium (III) and lanthanide (III) complexes containing 2, 2'-bipyridine with bovine serum albumin and their in vitro anticancer and antimicrobial activities.* Journal of Biomolecular Structure and Dynamics, 2020: p. 1-12.
56. El-Hady, A., et al., *Antibacterial and UV Protection Properties of Modified Cotton Fabric Using a Curcumin/TiO2 Nanocomposite for Medical Textile Applications.* Polymers, 2021. **13**(22): p. 4027.
57. Aramesh-Boroujeni, Z., et al., *Experimental and computational interaction studies of terbium (III) and lanthanide (III) complexes containing 2, 2'-bipyridine with bovine serum albumin and their in vitro anticancer and antimicrobial activities.* Journal of Biomolecular Structure and Dynamics, 2020: p. 1-12.